

# Mineral Mapping of FeO and TiO<sub>2</sub> of the Cassini crater using Moon Mineralogy Mapper (M3) of Chandrayaan – 1

Shashwat Shukla<sup>1</sup>, Shashi Kumar<sup>2</sup> and Shefali Agrawal<sup>3</sup>

<sup>1</sup>Geo-Informatics Dept., Indian Institute of Remote Sensing, Indian Space Research Organization, Dehradun

Email: [sshashwat93@gmail.com](mailto:sshashwat93@gmail.com)

<sup>2</sup>Photogrammetry and Remote Sensing Dept., Indian Institute of Remote Sensing, Indian Space Research Organization, Dehradun

Email: [shashi@iirs.gov.in](mailto:shashi@iirs.gov.in)

<sup>3</sup>Photogrammetry and Remote Sensing Dept., Indian Institute of Remote Sensing, Indian Space Research Organization, Dehradun

Email: [shefali\\_a@iirs.gov.in](mailto:shefali_a@iirs.gov.in)

**KEYWORDS:** Moon Mineralogy Mapper, Regolith, Optical Maturity, Optimized end member, Weight Percentage

**ABSTRACT:** An essential aspect of space exploration is the study of the geological makeup of any interplanetary body and the Moon has been a source of great fascination for scientific researchers in this field. Lunar surface mineralogy provides significant shreds of evidence for interpreting the composition and evolution of the planet's crust. Spectral changes due to perpetuated exposure of the planetary surface to the space environment could be quantified using geological remote sensing. These optical properties depend on relative rates of surface modification processes. Assessment of the measure of lunar soil evolution may be denoted in terms of Optical Maturity (OMAT). Optical maturity parameter is an indicator of the maturity of lunar regolith and hence, its estimation is of great importance in studying the geological characterization of the lunar surface. Also, lunar mineral exploitation may be of significant importance in the near future. Synergetic use of spectral reflectance of lunar surface acquired by Moon Mineralogy Mapper (M3), onboard Chandrayaan – 1, with a hypothetically hyper matured optimized end member of the data, along with the standard weight percentages of FeO and TiO<sub>2</sub> from lunar returned samples of Apollo and Luna landing sites, has been carried out using remote sensing based data interpolation techniques. The present work focusses on quantifying elemental concentration for characterizing lunar soil using hyperspectral data for Cassini crater, located at the eastern end of Mare Imbrium. Using local mosaic of M3 hyperspectral data and recalibrated element derivation algorithms, local modal abundance of FeO and TiO<sub>2</sub> is found to be 6.88 wt% and 3.59 wt% respectively. The overall results establish that the crater is highly matured with a local modal maturity index of 0.064.

## 1. INTRODUCTION

One of the most concerned studies in the field of inter planetary sciences is the accurate and efficient characterization of planetary surface for the identification of different types of minerals present, detection of water/ice deposits, automated crater boundary extraction, differentiating terrains, crater rim mapping, relative age estimation and surface morphological based studies. The Moon is a celestial body which revolves around the Earth. It is the Earth's only natural satellite and the fifth largest satellite in our solar system. It is different from the Earth in many ways, especially in terms of atmosphere, physical and chemical surface properties. It was formed at around 4.5 billion years ago. There are many theories involving the formation of the Moon. One of the theories states that it was formed due to a giant impact between Earth and another Mars sized body. The Moon is a rocky planetary object heavily cratered on the surface and flooded by lava flows. It was hit by meteors, comets and asteroids continuously, which led to the formation of regolith layer. Regolith can be termed as unconsolidated or loose rock material which more or less covers the entire surface or the underlying bedrock (Fa & Jin, 2010). The regolith layer contains information that is necessary in order to understand the surface and environment of the Moon (P. Lucey et al., 2006). Craters dominate all other features available on the Moon, other features being domes and cones, faults and graben. Our understanding of the lunar surface until now has been based on the data collected by various missions like the Galileo, Clementine and the lunar prospector and the samples of the regolith collected by missions like Apollo and

Luna. The Moon contains various resources for space and Earth, water ice, minerals and metals being some of them. The Moon contains a record of information pertaining to planetary history, evolution and processes (Spudis, Paul D). This information is not available on the Earth or elsewhere due to the dynamic processes which erode the surfaces continuously. So the study of moon surface helps to understand the early processes that contributed to the formation of the earth. The USSR and USA made attempts and sent a probe to moon began a new scientific era. As a result of this it made to possible to obtain high resolution images of moon and manned missions returned with lunar samples. The outermost layer of the lunar surface is known as Regolith and it is divided in to six categories namely mare, highlands, cratering, highland mare mixing, non-mare volcanism and tectonic features. Darker areas of the moon which can be seen through the naked eye are known as mare and is composed of basaltic lava flow. The high lands are made up of a silicate compound known as Anorthosite (mineral containing Calcium and Aluminum). Circular and semicircular features, which characterizes lunar surface are known as craters. Craters are holes in the ground, usually covering vast areas. They caused by a celestial body impacting another, volcanic activity, an underground explosion such as one caused by a nuclear weapon or a phreatic eruption, a sinking of the surface. Craters formed by celestial bodies are called impact craters. Volcanic activities can also form craters. In such instances, the craters are simply called volcanic craters or calderas. Volcanic craters, which usually come in the form of circular depressions, have very similar appearances to impact craters. The craters are usually formed during volcanic eruption empties the volcanoes magma chamber, consequently causing the area above it to collapse. Underground explosions, which form cavities there, also force the ground above it to collapse. Explosions caused by nuclear weapons are known as subsidence craters. On the other hand, if the explosion is the result of groundwater interacting with hot lava or magma, then the resulting crater is called a maar. The high land mare mixing are regions of the lunar surface, which formed due to mutual contact of the highlands and the mare. Non mare volcanism is recognized by volcanic rocks. Major minerals of lunar are Anorthosite Plagioclase, a compound composed of Calcium, Sodium, Aluminium, Silicon and Oxygen. Major compounds seen in this area are iron rich minerals like Pyroxene ( $(Ca\ Fe\ Mg)_2\ Si_2\ O_6$  Olivine ( $Fe\ Mg)_2\ Si\ O_4$  , Ilmenite etc (Senthil Kumar et al., 2011).

### 1.1. OPTICAL MATURITY PARAMETER (OMAT)

Optical maturity is a tool to measure the surface exposure of lunar soil based on the reflectance spectra. It gives approximate information about the birth of an object present in the surface of the Moon. Mathematically optical maturity is defined as the Euclidean distance from hypothetically fully matured (dark red) origin to the point of interest in terms of spectral reflectance (Paul G. Lucey, Blewett, & Jolliff, 2000). It is given as:

$$OMAT = [(R_{750} - x_0)^2 + \{(R_{950}/R_{750}) - y_0\}^2]^{1/2}$$

Where,

OMAT = Optical Maturity Index  
 $R_{750}$  = Mean Reflectance at 750 nm wavelength of the spectrum  
 $R_{950}$  = Mean Reflectance at 950 nm wavelength of the spectrum  
 $x_0$  = Reflectance of the Origin  
 $y_0$  =  $(R_{950}/R_{750})$  of the Origin

$(x_0, y_0)$  values are constant for a particular sensor (Blewett, Hawke, & Lucey, 2005; Paul G. Lucey, Blewett, & Jolliff, 2000). Since spectral reflectance is a rational value, optical maturity is a unit-less quantity. Optical maturity parameter can be used as a tool for lunar mapping (mineral mapping, soil mapping) etc., cratering studies (how craters are formed in lunar surface) and relative age dating (approximate age determination) (Blewett et al., 2005; Paul G. Lucey, Blewett, & Jolliff, 2000). Optical properties of lunar soil are controlled by OMAT parameter (Pieters, Shkuratov, Kaydash, Stankevich, & Taylor, 2006). Based on the optical maturity values lunar regolith can be classified in to three regions: mature, sub mature and immature.

### 1.2. ELEMENTAL ALGORITHM FOR FEO MAPPING

M3 provides hyperspectral data of the moon with a spatial resolution of 140 m/pixel. This data is very much useful to map the iron oxide on the lunar surface. Ferrous oxide is one of the components of major silicates present on the lunar surface. Lunar mineral reflectance spectra reveal ferrous iron containing minerals show high reflectance

around 750 nm regions and low reflectance around 950 nm region of the electromagnetic spectrum. To map the ferrous oxide in the lunar surface initially ferrous iron sensitive parameter is generated. Lucey et al developed a remote sensing method to find out the ferrous iron content in the lunar surface by deriving an angular parameter to locate the iron content in the lunar regolith (P. G. Lucey, Taylor, & Malaret, 1995). Lucey et al., plotted the 750 nm reflectance values against (950/750) nm reflectance values and determined the hypothetical matured origin. Based on the origin an angular parameter sensitive to iron was derived. The angular parameter is known as Iron sensitive parameter  $\Theta_{Fe}$ .

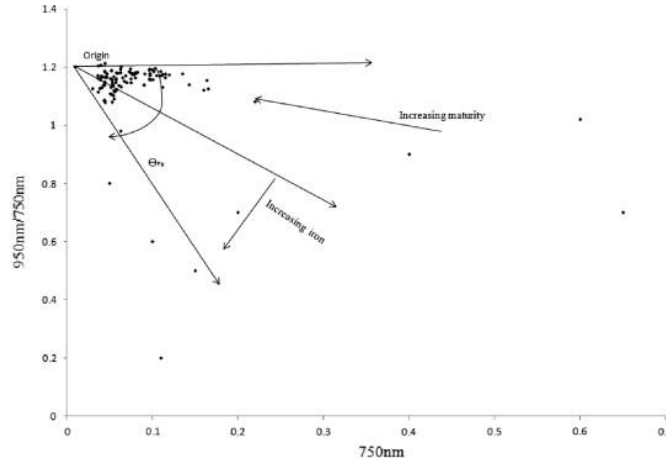


Fig 1. Graphical representation of sensitive parameter (P. G. Lucey et al., 1995)

From the figure, iron sensitivity parameter is defined as the angle between horizontal line through the origin and the line defined by the origin and the desired location on the image plane.

This angular parameter aligns the iron reflectance regions around the angle  $\Theta_{Fe}$ . Lucey defined  $\Theta_{Fe}$  for iron mathematically as follows:

$$\Theta_{Fe} = -\tan^{-1}[\{(R_{950}/R_{750}) - y_0\} / (R_{750} - x_0)]$$

Where  $(x_0, y_0)$  represents the optimized origin and  $R_{950}$  &  $R_{750}$  represents reflectance at 950 nm and 750 nm respectively (Paul G Lucey, David, & Hawke, 1998). Correlation coefficient of FeO content of Apollo mission returned samples and iron sensitivity parameter shows good correlation. Reflectance and band ratio values corresponding to the maximum correlation coefficient is taken as origin. Linear regression fitting is used to generate weight percentage equation for FeO. This best fit polynomial gives the weight percentage of FeO and is given by:

$$\text{Wt\% FeO} = 17.42 * \Theta_{Fe} - 7.565$$

(Paul G. Lucey, 2000)

This polynomial equation may change according to different sensors.

### 1.3. ELEMENTAL ALGORITHM FOR TiO<sub>2</sub> MAPPING

In a similar way as FeO weight percentage calculated, TiO<sub>2</sub> weight percentage is calculated. For this sensitive parameter for Ti is generated using UV region wavelength (415 nm) and the (415/750) nm ratio. Sensitive parameter for Ti is given as:

$$\Theta_{Ti} = \tan^{-1}[\{(R_{415}/R_{750}) - y_0\} / (R_{750} - x_0)]$$

(Lucey, 2000; Wohler, 2011)

Where  $(x_0, y_0)$  represents the optimized origin and  $R_{415}$  &  $R_{750}$  represents reflectance at 415 nm and 750 nm respectively.  $\text{TiO}_2$  content from lunar sample sites were collected and correlation between  $\text{TiO}_2$  and  $\Theta_{\text{Ti}}$  was found. Weight percentage of  $\text{TiO}_2$  was found out using second order polynomial fit between  $\Theta_{\text{Ti}}$  and  $\text{TiO}_2$ . As UV range is directly not available in the prescribed range for Chang 'E-1 2M Lucey modified the formula as follows:

$$\Theta_{\text{Ti}} = \tan^{-1}[\{(R_{561}/R_{750}) - y_0\} / (R_{750} - x_0)]$$

(Wu et al., 2012)

The same method can be adopted in the case of M3 data; instead of 415 nm, 540 nm band is selected.

## 2. DATASET AND STUDY AREA

Recalibration of the classical method for mineral content estimation of the lunar regolith is performed using hyperspectral data from M3 sensor. M3, the guest sensor of Chandrayaan-1 provides data in Global and Target modes. NASA level 1B, spectral radiance data acquired by M3 in Global mode have been used for this recalibration work. M3 level 1B data format is 32 bit floating point and image format is Band Interleaved by Line (BIL) with an average image size of 2.8 GB. Each M3 strip provides pole to pole coverage in a comparatively narrow width and hence several such strips are required to cover a big crater or an impact basin of the lunar regolith. The study area chosen is Cassini crater, located in the Palus Nebularum, at the eastern end of Mare Imbrium, with selenographic coordinates  $(40.2^\circ \text{ N}, 4.6^\circ \text{ E})$  shown in the Figure 2. The floor of Cassini is flooded, and is likely as old as the surrounding mare.

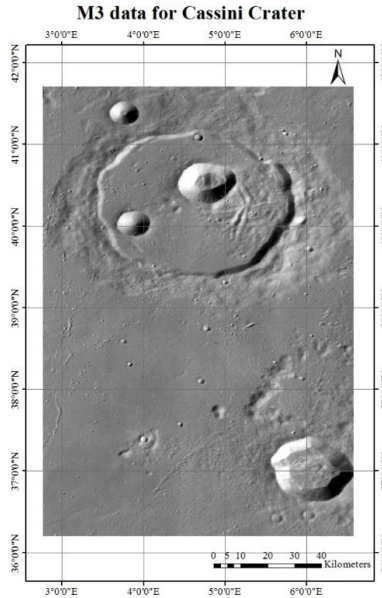


Figure 2. Study area of M3 dataset

## 3. METHODOLOGY

The methodology adopted to achieve the objective of the study is shown in Figure 3. Lunar surface characterization for the retrieval of mineral parameter is mainly divided into three parts: Origin optimization, lunar optical maturity estimation and Sensitive parameter determination. Recalibration of the classical work of Lucey and Coworkers, was done with M3 global data and derived the hypothetically hyper matured origin for FeO and  $\text{TiO}_2$  estimation. Equations were generated for the best fitting regression curve of Fe and Ti sensitive parameters with respect to the weight percentages of the elemental mineral concentrations determined for Apollo and Luna landing sites.

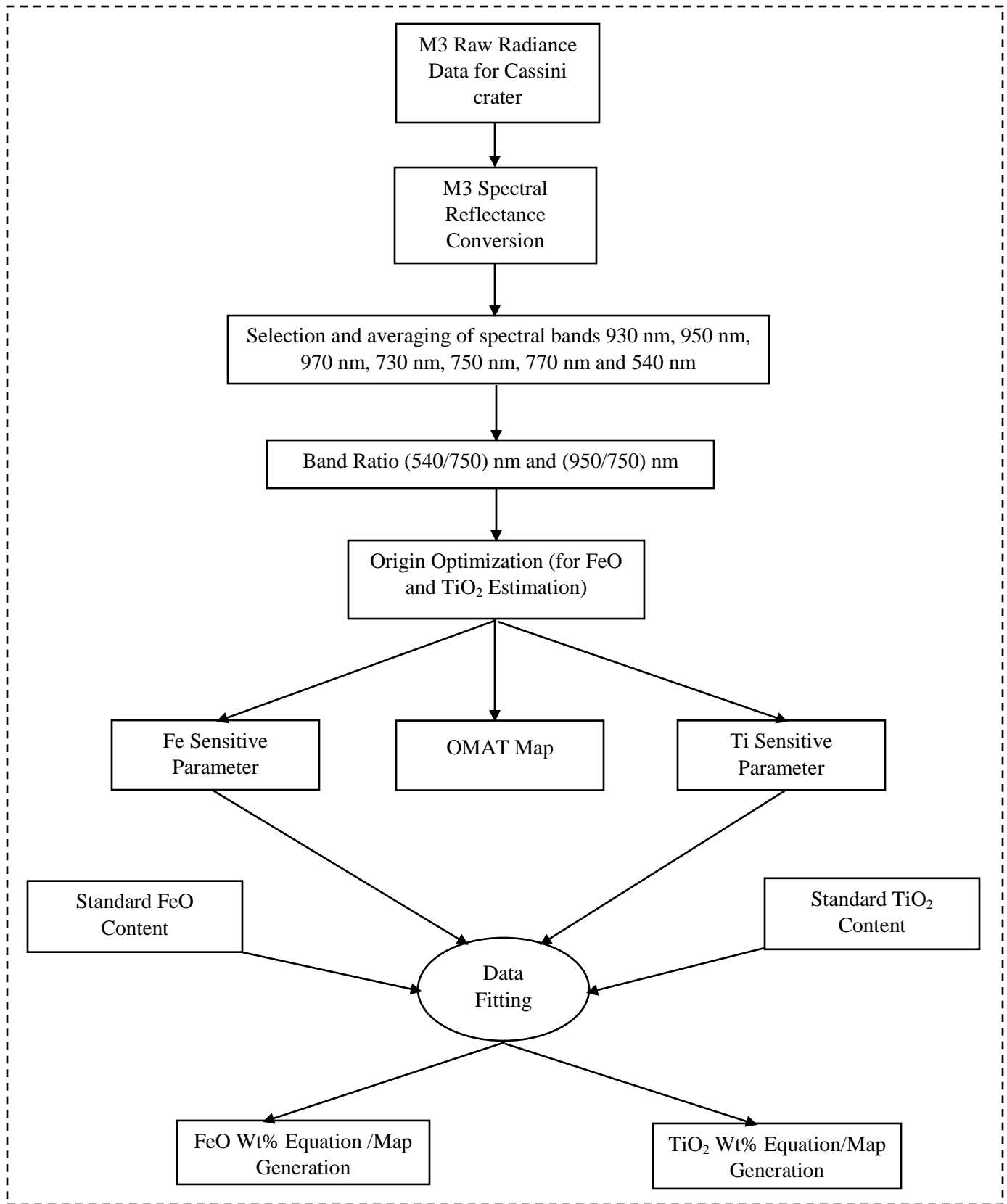


Figure 3. Proposed Methodology for the mineral content retrieval

## 4. RESULTS AND DISCUSSIONS

### 4.1. Optical Maturity (OMAT) for Lunar Soil

Optical maturity, a measurement tool of degree of maturation, is defined as the Euclidian distance from the optimized origin to the desired location on the image. Optical maturity of Cassini crater from M3 data strip are represented in Figure 4.1. OMAT of the processed area varies approximately from 0.001068 to 0.552232 with a mean value of 0.075403, which indicates that the crater is highly matured.

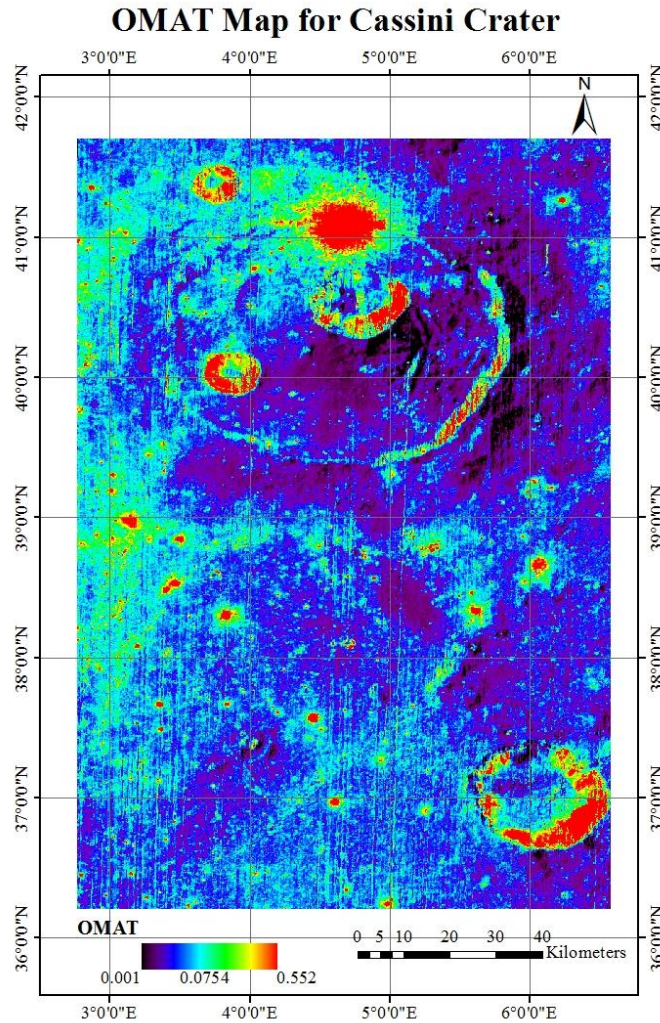


Figure 4.1. OMAT of Cassini Crater

### 4.2. FeO Estimation for Cassini Crater

FeO estimation of Cassini crater from M3 data strip are represented in Figure 4.2. FeO of the processed area varies approximately from 4.715312% to 16.72% with a mean value of 7.38476%.

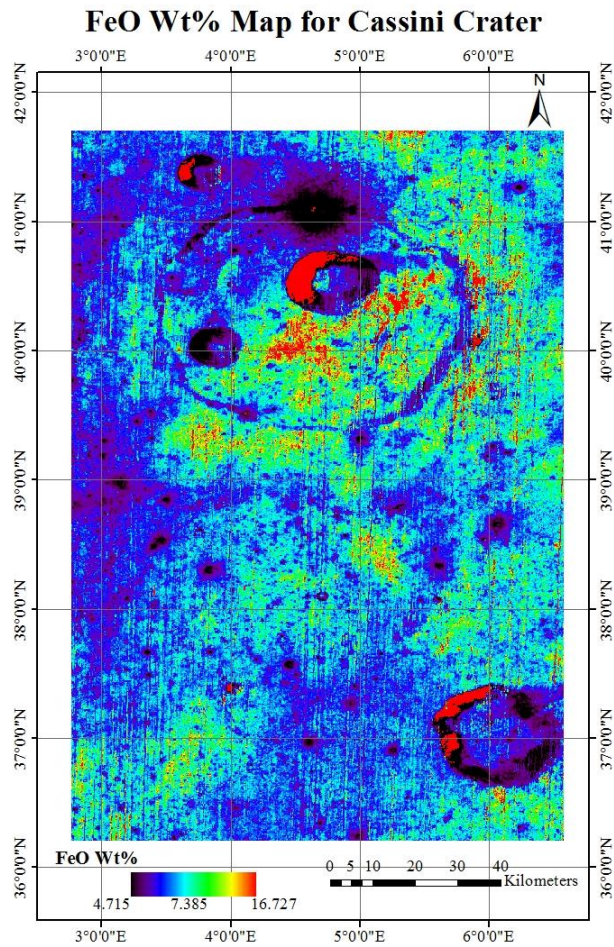


Figure 4.2. FeO Wt% Estimation of Cassini Crater

FeO weight percentage equations are generated from sensitive parameters and standard FeO contents of the Apollo and Luna landing sites using linear regression fit. Results of linear regression fit are given in Figure 4.3. Equation of the best fit line with optimum correlation coefficient is treated as the weight percentage equation for FeO estimation.

Linear regression equation of the best fit line with an  $R^2$  value of 0.53 given below is treated as the M3 FeO weight percentage equation.

$$\text{FeO Wt\%} = 0.0667 \Theta_{\text{Fe}} + 10.721$$

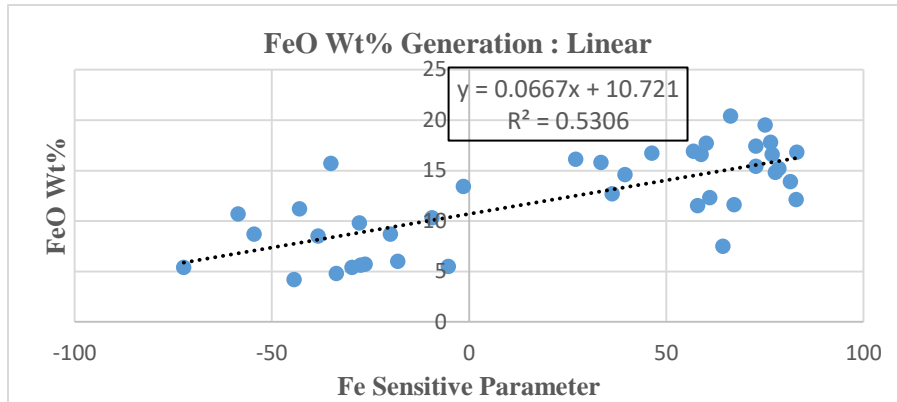


Figure 4.3. FeO Wt% Generation

#### 4.1.3. TiO<sub>2</sub> Estimation for Cassini Crater

TiO<sub>2</sub> estimation of Cassini crater from M3 data strip are represented in Figure 4.5. TiO<sub>2</sub> of the processed area varies approximately from 3.455370% to 3.647314% with a mean value of 3.57%. TiO<sub>2</sub> weight percentage equations are generated from sensitive parameters and standard TiO<sub>2</sub> contents of the Apollo and Luna landing sites using exponential regression fit. Results of linear regression fit are given in Figure 4.4. Equation of the best fit line with optimum correlation coefficient is treated as the weight percentage equation for TiO<sub>2</sub> estimation.

Exponential regression equation of the best fit line with an  $R^2$  value of 0.53 given below is treated as the M3 TiO<sub>2</sub> weight percentage equation.

$$\text{TiO}_2 \text{ Wt\%} = 1.8831e^{-0.005 \Theta_{\text{Ti}}}$$

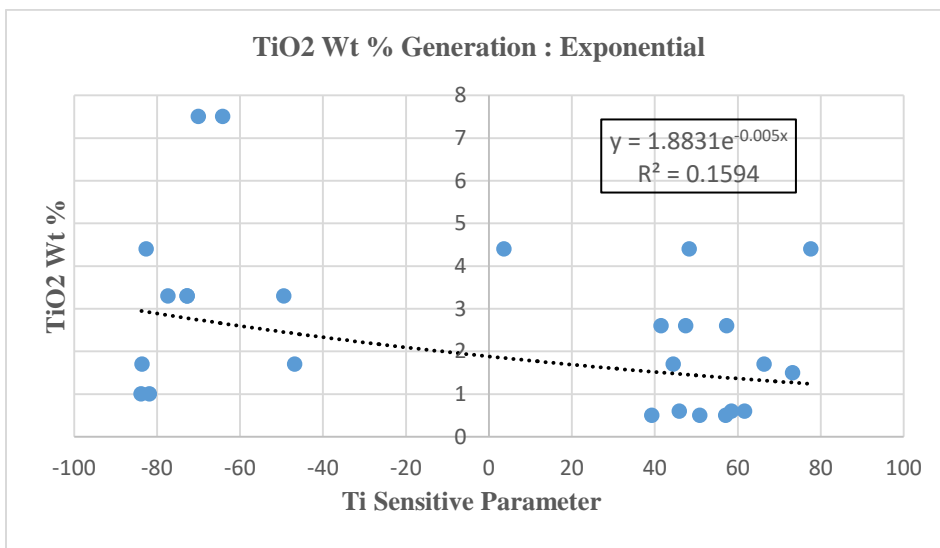


Figure 4.4. Exponential TiO<sub>2</sub> Wt% Generation

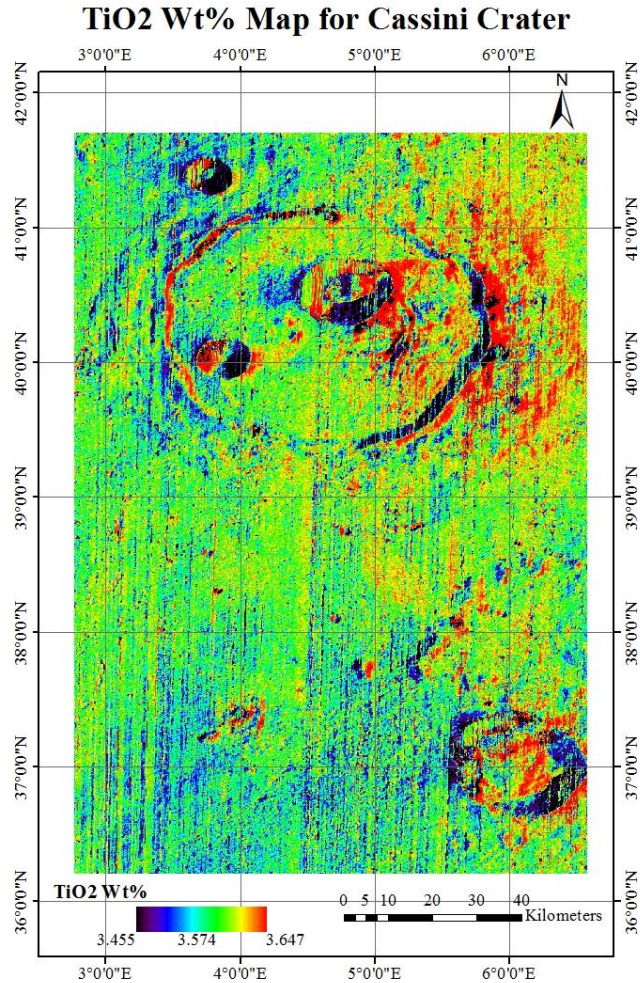


Figure 4.5.  $\text{TiO}_2$  Wt% Map for Cassini Crater

## 5. CONCLUSION

In this study, an attempt has been made to estimate the elemental mineral concentration by determining the optical maturity of the lunar soil of Cassini crater, located in the Palus Nebularum, at the eastern end of Mare Imbrium. The present work quantifies mineral content using hyperspectral data by reproducing the work of P. G. Lucey et al., 1995; 1998; 2000 and Blewett et al., 2005, 1997. Using remote sensing based data interpolation techniques, integrated use of spectral reflectance of lunar surface acquired by Moon Mineralogy Mapper (M3), onboard Chandrayaan – 1, with a hypothetically hyper matured optimized end member of the data has been carried out. By utilizing the standard weight percentages of FeO and  $\text{TiO}_2$  from lunar returned samples of Apollo and Luna landing sites, equations were generated by considering sensitive parameters. Using local mosaic of M3 hyperspectral data and recalibrated element derivation algorithms, local modal abundance of FeO and  $\text{TiO}_2$  is found to be 6.88 wt% and 3.59 wt% respectively. The overall results establish that the crater is highly matured with a local modal maturity index of 0.064.

## 6. REFERENCES

- Blewett, D. T., Hawke, B. R., & Lucey, P. G. (2005). Lunar optical maturity investigations: A possible recent impact crater and a magnetic anomaly. *Journal of Geophysical Research*, *110*(E4), E04015. <https://doi.org/10.1029/2004JE002380>
- Blewett, D. T., Lucey, P. G., Hawke, B. R., & Jolliff, B. L. (1997). Clementine images of the lunar sample-return stations: Refinement of FeO and TiO<sub>2</sub> mapping techniques. *Journal of Geophysical Research: Planets*, *102*(E7), 16319–16325. <https://doi.org/10.1029/97JE01505>
- Fa, W., & Jin, Y. Q. (2010). A primary analysis of microwave brightness temperature of lunar surface from Chang-E 1 multi-channel radiometer observation and inversion of regolith layer thickness. *Icarus*, *207*(2), 605–615. <https://doi.org/10.1016/j.icarus.2009.11.034>
- Lucey, P. G., Blewett, D. T., & Hawke, B. R. (1998). Mapping the FeO and TiO<sub>2</sub> content of the lunar surface with multispectral imagery. *Journal of Geophysical Research: Planets*, *103*(E2), 3679–3699. <https://doi.org/10.1029/97JE03019>
- Lucey, P. G., Blewett, D. T., & Jolliff, B. L. (2000). Lunar iron and titanium abundance algorithms based on final processing of Clementine ultraviolet-visible images. *Journal of Geophysical Research: Planets*, *105*(E8), 20297–20305. <https://doi.org/10.1029/1999JE001117>
- Lucey, P. G., Blewett, D. T., Taylor, G. J., & Hawke, B. R. (2000). Imaging of lunar surface maturity. *Journal of Geophysical Research: Planets*, *105*(E8), 20377–20386. <https://doi.org/10.1029/1999JE001110>
- Lucey, P. G., David, T. B., & Hawke, B. R. (1998). Mapping the FeO and TiO<sub>2</sub> content of the lunar surface with multispectral imagery. *Journal of Geophysical Research*, *103*(E2), 3679–3699. <https://doi.org/10.1029/97JE03019>
- Lucey, P. G., Taylor, G. J., & Malaret, E. (1995). Abundance and Distribution of Iron on the Moon. *Science*, *268*(5214), 1150–1153. <https://doi.org/10.1126/science.268.5214.1150>
- Lucey, P., Korotev, R. L., Gillis, J. J., Taylor, L. A., Lawrence, D., Campbell, B. A., ... Maurice, S. (2006). Understanding the Lunar Surface and Space-Moon Interactions. *Reviews in Mineralogy and Geochemistry*, *60*(1). Retrieved from <http://ring.geoscienceworld.org/content/60/1/83>
- Pieters, C., Shkuratov, Y., Kaydash, V., Stankevich, D., & Taylor, L. (2006). Lunar soil characterization consortium analyses: Pyroxene and maturity estimates derived from Clementine image data. *Icarus*, *184*(1), 83–101. <https://doi.org/10.1016/j.icarus.2006.04.013>
- Senthil Kumar, P., Senthil Kumar, A., Keerthi, V., Goswami, J. N., Gopala Krishna, B., & Kiran Kumar, A. S. (2011). Chandrayaan-1 observation of distant secondary craters of Copernicus exhibiting central mound morphology: Evidence for low velocity clustered impacts on the Moon. *Planetary and Space Science*, *59*(9), 870–879. <https://doi.org/10.1016/j.pss.2011.04.004>
- Spudis, P. D. (n.d.). Introduction to the Moon, Moon 101.
- Wohler, C., Berezhnoy, A., & Evans, R. (2011). Estimation of elemental abundances of the lunar regolith using clementine UVVIS+NIR data. *Planetary and Space Science*, *59*(1), 92–110. <https://doi.org/10.1016/j.pss.2010.10.017>
- Wu, Y., Xue, B., Zhao, B., Lucey, P., Chen, J., Xu, X., ... Ouyang, Z. (2012). Global estimates of lunar iron and titanium contents from the Chang' E-1 IIM data. *Journal of Geophysical Research: Planets*, *117*(E2), n/a-n/a. <https://doi.org/10.1029/2011JE003879>